Mon. Not. R. Astron. Soc. **345,** 949–959 (2003)

UBRI photometry of globular clusters in the Leo group galaxy NGC 3379

Shannon Whitlock,★ Duncan A. Forbes★ and Michael A. Beasley★
Centre for Astrophysics & Supercomputing, Swinburne University, Hawthorn, VIC 3122, Australia

Accepted 2003 July 14. Received 2003 July 11; in original form 2003 May 8

ABSTRACT

We present wide-area *UBRI* photometry for globular clusters around the Leo group galaxy NGC 3379. Globular cluster candidates are selected from their *B*-band magnitudes and their $(U - B)_o$ versus $(B - I)_o$ colours. A colour–colour selection region was defined from photometry of the Milky Way and M31 globular cluster systems. We detect 133 globular cluster candidates, which supports previous claims of a low specific frequency for NGC 3379.

The Milky Way and M31 reveal blue and red subpopulations, with $(U - B)_o$ and $(B - I)_o$ colours indicating mean metallicities similar to those expected based on previous spectroscopic work. The stellar population models of Maraston and Brocato et al. are consistent with both subpopulations being old, and with metallicities of [Fe/H] ~ -1.5 and -0.6 for the blue and red subpopulations, respectively. The models of Worthey do not reproduce the $(U - B)_o$ colours of the red (metal-rich) subpopulation for any modelled age.

For NGC 3379 we detect a blue subpopulation with similar colours, and presumably age/metallicity, to that of the Milky Way and M31 globular cluster systems. The red subpopulation is less well defined, perhaps due to increased photometric errors, but indicates a mean metallicity of [Fe/H] ~ -0.6.

Key words: globular clusters: general – galaxies: individual: NGC 3379 – galaxies: star clusters.

1 INTRODUCTION

In the last few years, it has become clear that globular cluster (GC) systems have complex colour distributions, indicating two or more subpopulations within a single elliptical galaxy (Ashman & Zepf 1992; Secker et al. 1995; Whitmore et al. 1995; Geisler, Lee & Kim 1996; Forbes, Brodie & Huchra 1997; Bridges et al. 1997; Kissler-Patig & Gebhardt 1998; Kundu & Whitmore 2001; Larsen et al. 2001). The subpopulations have different metallicities and possibly ages, indicating multiple epochs or mechanisms of formation. As GCs are thought to trace the star formation and chemical enrichment episodes of their host galaxy (e.g. Forbes & Forte 2001), understanding how they formed will provide important constraints on the process of galaxy formation and evolution. The main scenarios for GC formation include the following.

(i) The merger of two gas-rich (spiral) galaxies may lead to the formation of an elliptical galaxy and create an additional population of GCs in the process (Ashman & Zepf 1992). As the GCs produced in the merger formed from enriched gas they should be of higher metallicity and thus redder than the indigenous (metal-poor) GC population. Thus we expect a metal-poor old population (∼13 Gyr) plus a metal-rich young population with an age similar to that of the merger itself.

(ii) A multi-phase collapse (Forbes et al. 1997) can also produce two distinct GC populations. Here the blue GCs formed in an early chaotic phase of galaxy formation from metal-poor gas and the red GCs form later from enriched gas in the same phase that produces the bulk of the galaxy starlight. A multi-phase collapse also predicts an old metal-poor subpopulation and one slightly younger (Δ age ∼2–4 Gyr) metal-rich one.

(iii) Cote, Marzke & West (1998) describe the build-up of the GC systems of bright ellipticals via the accretion of mostly metal-poor GCs from dwarf galaxies. In this picture the metal-rich GCs are indigenous and the metal-poor ones are acquired. Here both the GC subpopulations will be about the same age (i.e. old) but have different metallicities.

(iv) Formation of GC systems in hierarchical merging is described in Beasley et al. (2002). In this prescription blue GCs form in pre-galactic clumps. These gaseous clumps merge generating a second generation of red GCs, along with galactic star formation. Late stage mergers of more stellar clumps may include accreted GCs. Thus the hierarchical picture contains elements of the other three. In a hierarchical universe, the metal-poor GCs will be old and the the metal-rich GCs will have a mean age that depends on galaxy mass and environment.

Perhaps the best direct test of these competing GC formation models is to determine the mean age and metallicity of the GC

★E-mail: swhitlock@swin.edu.au (SW); dforbes@astro.swin.edu.au (DAF); mbeasley@astro.swin.edu.au (MAB)

subpopulations for a large number of galaxies. In principle, the best way to do this is from GC spectra. Indeed this is an active area of research, using the world largest telescopes, and is returning exciting new results (e.g. Kissler-Patig et al. 1998; Forbes et al. 2001; Larsen et al. 2002; Beasley et al. 2003). However, it is also very time-consuming. Photometry is more efficient, but optical colours suffer from the well-known age–metallicity degeneracy. This situation can be improved by extending photometry to the near-infrared (e.g. Puzia et al. 2002) or ultraviolet. Photometry in the U (3600 Å) band is very rare for GC systems beyond the Local Group (the ∼70 GCs in NGC 5128 with U-band photometry from Rejkuba 2001 is one exception). This is largely due to the poor blue response of most CCDs in use today and the low fraction of U-band light emitted by old stellar populations such as GCs.

Here we present *UBRI* photometry of GCs associated with the Leo Group galaxy NGC 3379, obtained with the blue-sensitive CCDs of the Isaac Newton Telescope 2.5-m Wide Field Camera. By extending the traditional optical photometry to bluer U-band wavelengths, we can better probe the metallicity distribution of the GC system in NGC 3379. We also utilize some smaller field-of-view images taken with the Gemini North 8-m telescope to aid in the selection of GC candidates.

NGC 3379 (M105) is a moderate luminosity E1 galaxy in the nearby ($D = 11.5$ Mpc, $m - M = 30.30$) Leo Group. In a photographic study of NGC 3379, Harris & van den Bergh (1981) estimated a total GC population of 290 ± 150. This translates into a low specific frequency S_N of 1.1 ± 0.6 (assuming $M_V = -21.06$). Ajhar, Blakeslee & Tonry (1994) obtained VRI CCD images of NGC 3379, detecting some 60 GCs. However, they did not detect any obvious bimodality in the GC colour distribution. The first clear detection of bimodality came from the *Hubble Spcae Telescope* (*HST*) study by Larsen et al. (2001). They found peaks at $(V - I)_o = 0.96$ and 1.17 for the blue and red subpopulations, respectively.

2 OBSERVATIONS AND DATA REDUCTION

Broad-band *UBRI* images covering the Leo galaxies NGC 3379, 3384 and 3389 were obtained using the 2.5-m Isaac Newton Telescope (INT) on 2000 February 6 and 8. The Wide Field Camera (WFC) comprises four thinned EEV 4096 × 2048 CCDs, with pixels of 0.33 arcsec and provides a field-of-view of approximately 30 × 30 arcmin^2. Observing conditions were photometric over the two nights with seeing of 1.5 arcsec in the U- and I-bands and 2.2 arcsec in the B- and R-bands. The total exposure times were roughly 2000 (U), 3000 (B), 1500 (R) and 1000 s (I). In addition to the galaxy observations, several standard star fields from Landolt (1992) were obtained over both the nights that bracket the galaxy observations.

Basic data reduction was performed using IRAF and specially written software by A. Terlevich. This consisted of master bias subtraction, non-linear correction, flat-fielding using combined sky flats, alignment and co-addition of individual frames. The galaxy frames and standard stars were reduced in an identical manner. Raw magnitudes of between 10 and 30 stars were obtained for each filter using the IRAF task QPHOT, after determining the optimal aperture size. The zero-point for each filter was determined by a simple linear fit to the stellar raw magnitudes versus stellar colour and a correction for airmass. The airmass extinction coefficients of $K_U = 0.46$, $K_B = 0.22$, $K_R = 0.08$ and $K_I = 0.04$ mag/airmass have been taken from the INT WFC web page. The final airmass-corrected, 1-s zero-points are $Z_U = 22.98 \pm 0.01$, $Z_B = 24.84 \pm 0.02$, $Z_R = 24.65 \pm 0.02$ and $Z_I = 23.96 \pm 0.01$. The BRI zero-points compare well with those determined by Miles et al. (in preparation) from the same observing run and the zero-points listed on the INT/WFC web-page. An independent estimate of the U-band zero-point ($Z_U = 22.98 \pm 0.05$) was made by F. Reda (private communication) by comparing various aperture magnitudes for NGC 3379 to that listed in Hypercat (http://www-obs.univ-lyon1.fr/hypercat/). Finally, we adjusted these zero-points for Galactic extinction using values from the NASA Extragalactic Data base (http://ned.ipac.caltech.edu), i.e. $A_U = 0.132$, $A_B = 0.105$, $A_R = 0.065$, $A_I = 0.047$.

3 GALAXY MODELLING

In order to better reveal the inner GCs, we subtracted a model of NGC 3379. Galaxy subtraction was performed using the STSDAS ISOPHOTE package (see Forbes & Thomson 1992). A galaxy model, with a varying centre, ellipticity and position angle, was fitted in all four filters. Isophotes were modelled out to ∼350 arcsec (20 kpc). A 3σ clip criterion over five iterations was used to remove deviant pixels (e.g. bright objects) from the fit. The model-subtracted images were visually inspected and iterated if necessary to provide a smooth transition from the background level to the model-subtracted region. The resulting residual images made it easier to identify the inner GCs.

4 INITIAL OBJECT FINDING AND SELECTION

The four filter (i.e. *UBRI*) images of the Leo galaxy triplet were aligned to within a fraction of a pixel and trimmed using the IMALIGN task. We then used DAOFIND to select GC candidates in each filter independently. Selection criteria consisted of a signal-to-noise ratio (S/N) threshold of 6 and a point-spread function full width at half maximum (PSF FWHM) adjusted to the seeing conditions in each filter. Additionally, roundness criteria ranging between values of −1.0 and 1.0 and a sharpness range of 0 to 1.0 provided good exclusion of extended objects. The resulting data base of GC candidates consisted of over 3000 objects for each filter. The PHOT task was used to measure the magnitude and error of each object in all four bands as found by DAOFIND. A simple script was written to perform the first stage of filtering and reduce the number of candidates to only those detected in all four bands. This spatial coordinate matching reduced the data set to 1200 objects with measured *UBRI* magnitudes. The same script determined galactocentric coordinates for each object based on the galaxy centre taken from the galaxy model (with the centre position constant within a fraction of a pixel). The reduced candidate list was then visually inspected to eliminate the small number of remaining galaxy-like extended objects or CCD artefacts.

5 MILKY WAY AND M31 GLOBULAR CLUSTER COLOURS

To aid in the selection and interpretation of Leo group GCs, we use observations of Milky Way and M31 GCs (essentially the only two galaxies that have well-studied GC systems in the U-band). Data for the Milky Way GC system comes from the compilation of Harris (1996). From this list, de-reddened U-, B- and I-band photometry exists for 95 GCs. Data for the M31 GC system come from Barmby et al. (2000). De-reddened magnitudes for 148 GCs were supplied

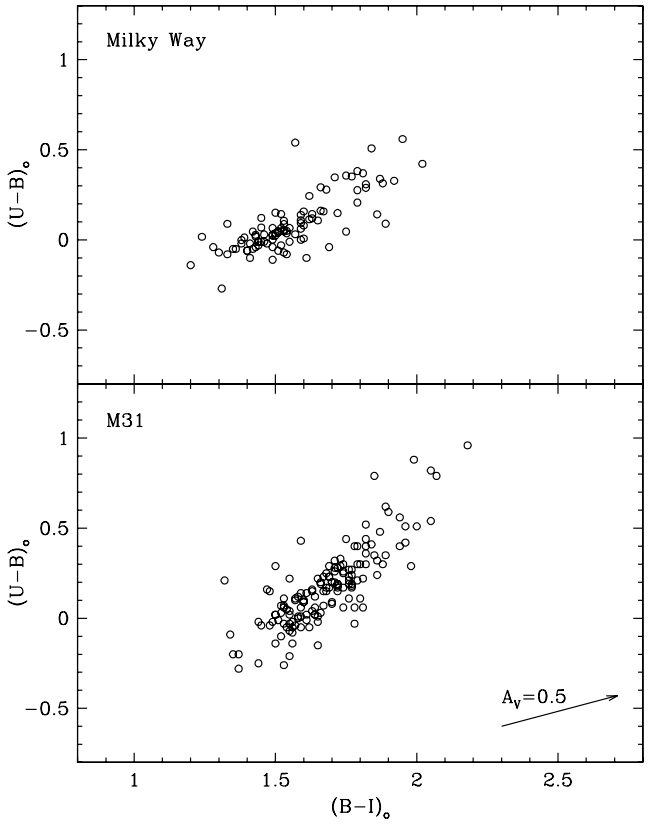

Figure 1. $(U - B)_o$ versus $(B - I)_o$ colour distribution for the Milky Way (top) and M31 (lower) GCs. The distribution for the two galaxies are similar, although they have slightly different slopes. The effect of 0.5 mag of extinction in the V band is also shown.

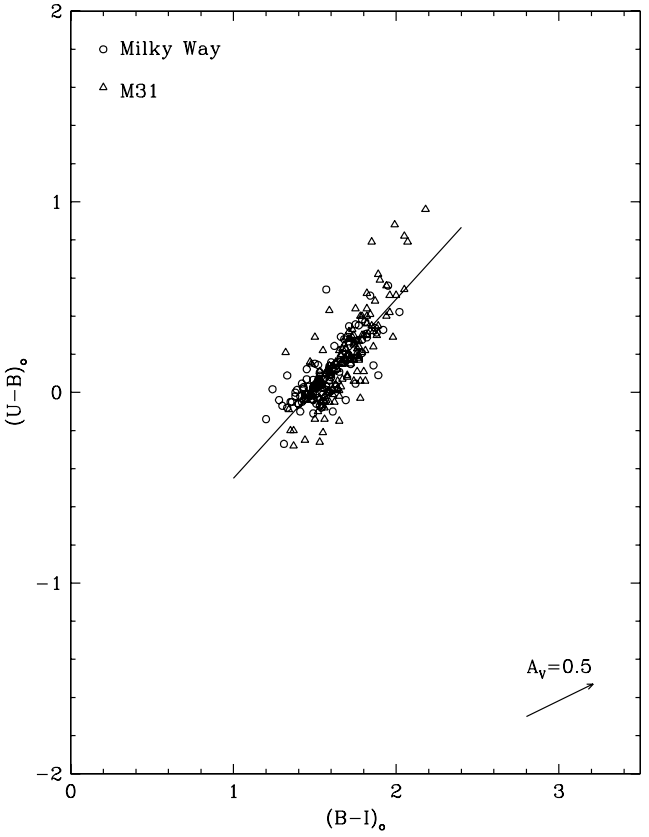

Figure 2. $(U - B)_o$ versus $(B - I)_o$ colour distribution for the combined Milky Way (circles) and M31 (triangles) GC samples. A least-squares fit to the combined sample is also shown. The best-fitting line is of the form $(U - B)_o = 0.94 \times (B - I)_o - 1.39$, with an rms spread about the best fit of ~ 0.12 mag.

by Barmby (private communication). In Fig. 1 we show the $(U - B)_o$ versus $(B - I)_o$ colour distribution for the Milky Way and M31 GC systems. To our knowledge this is the first time the $(U - B)_o$ versus $(B - I)_o$ colour distribution for the GCs of these galaxies have been examined together.

The data define a relatively tight distribution in this plot covering a range of $\sim$1.5 mag in each colour, with the M31 GCs extending to slightly redder colours. In general, the distributions for the two galaxies are qualitatively similar. However, we do note that the slope of the Milky Way distribution, $(U - B)_o = 0.725 \times (B - I)_o - 1.047$ (rms = 0.088), is somewhat flatter than that for M31, $(U - B)_o = 1.202 \times (B - I)_o - 1.850$ (rms = 0.122). This may represent intrinsic differences in the GC systems of the two galaxies, but is more likely to be due to the uncertain reddening corrections that have been applied. Both galaxies reveal a dominant grouping of blue GCs, with a less well-defined tail to redder colours. We associate the former with the metal-poor GC subpopulation and the latter with the metal-rich GC subpopulation in these galaxies. The location of these subpopulations in colour space will be discussed in more detail below. Noting the general similarities of the two distributions, we have combined the Milky Way and M31 GC samples to define a mean GC colour–colour distribution. This is shown in Fig. 2. A least-squares fit to the combined sample is also shown. The best-fitting line is of the form $(U - B)_o = 0.94 \times (B - I)_o - 1.39$, with an rms spread about the best fit of $\sim$0.12 mag. We use this colour–colour relation and spread to help us define the colours expected for GCs in NGC 3379.

6 GLOBULAR CLUSTERS IN THE CENTRAL REGION OF NGC 3379

Images of the central regions of NGC 3379 have been taken with the GMOS instrument on the Gemini North Telescope in 2003 February. Three fields, each covering 5 arcmin near the galaxy centre, were observed as shown in Fig. 3. These images, in Sloan filters g', r' and i', form the pre-acquisition imaging for an upcoming spectroscopic run. As they were obtained under excellent seeing conditions ($\sim$0.7 arcsec) the expected contamination rates for candidate GCs based on the Gemini data will be significantly less than for the INT data (obtained under $\sim$2-arcsec seeing). Candidate GCs from the Gemini data have been selected on the basis of their size (i.e. compactness) and colour ($0.5 < g' - i' < 1.5$ and $0.3 < g' - r' < 1.0$) by Faifer & Forte (private communication).

By spatially matching the Gemini object list with the initial INT object list (described above), we identified 125 matches. In Fig. 4 we show a colour–magnitude diagram for these Gemini-selected objects, with magnitudes taken from our INT photometry. Next we restricted the object list in B magnitude. An upper limit of $B = 19$ was chosen to exclude bright stars and/or compact dwarf galaxies. This limit is 4σ brighter than the expected GC turnover magnitude for NGC 3379, and corresponds to $M_B = -11.3$. We also imposed a lower magnitude cut-off of $B = 23$, to avoid any colour bias in the sample. These selection criteria are also shown in Fig. 4.

The resulting subset in a $(U - B)_o$ versus $(B - I)_o$ colour–colour diagram is shown in Fig. 5. This figure also shows the region

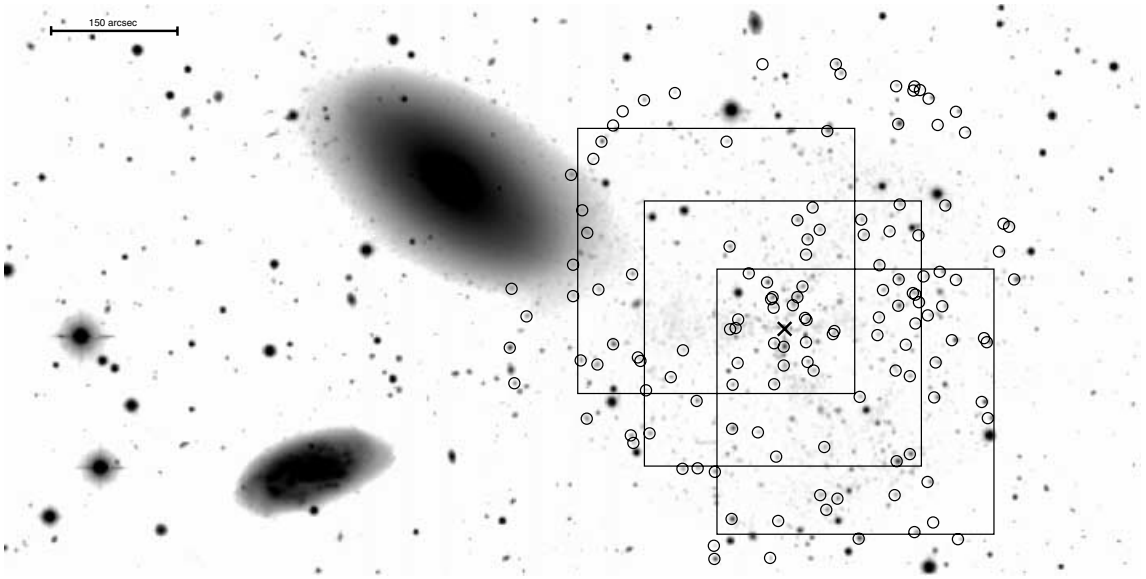

Figure 3. Grey-scale image of the Leo triplet field from the INT/WFC. NGC 3379 has been modelled and subtracted with its centre indicated by a cross. Small circles represent globular cluster candidates. The three large squares indicate the three regions covered by the Gemini/GMOS imaging. North is up and east is to the left. A 150-arcsec (8.4 kpc) size scale is shown.

of expected colours for GCs. The region ranges from $1.0 < (B - I)_o < 2.4$, and within 0.7 mag in $(U - B)_o$ of the mean Milky Way plus M31 fit. The $(B - I)_o$ range was chosen to be similar to that of the Milky Way and M31, i.e. covering the full metallicity range expected of GCs but allowing for an additional 0.25 mag in A_V reddening. The range in $(U - B)_o$ corresponds to the scatter seen

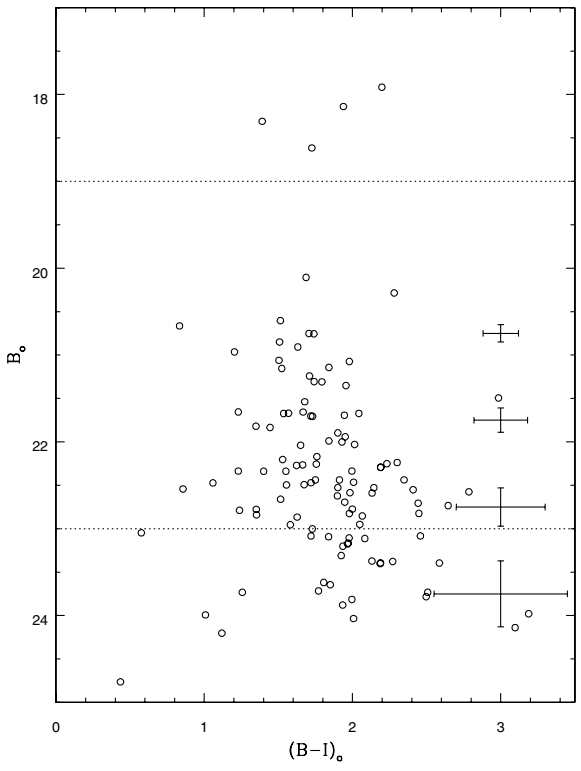

Figure 4. Colour–magnitude diagram for the candidate GCs from Gemini/GMOS images, using magnitudes from the INT/WFC. The expected GC turnover magnitude for NGC 3379 at a distance modulus of $m - M = 30.30$ is $B_o = 23.5$. The data show a hint of bimodality at $(B - I)_o \sim 1.6$ and 1.9. The dashed lines indicate the upper and lower magnitude cuts applied to this sample.

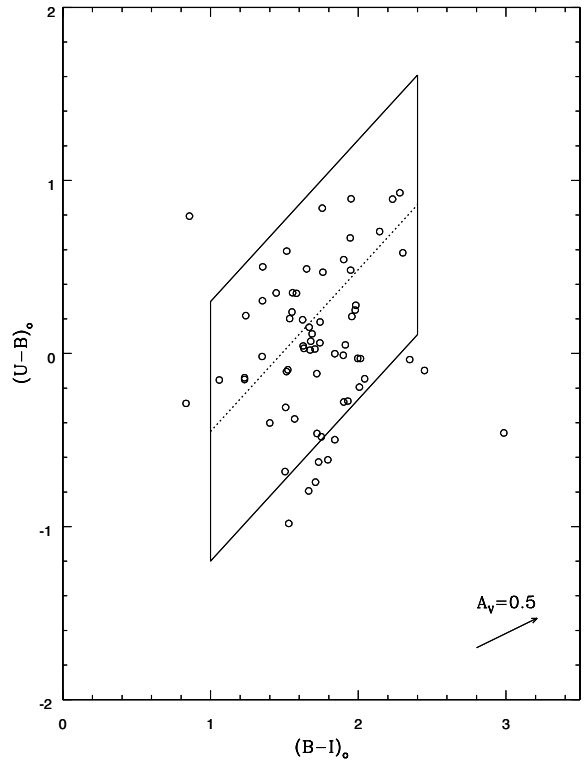

Figure 5. $(U - B)_o$ versus $(B - I)_o$ colour distribution for the candidate GCs selected from Gemini/GMOS images, after applying spatial matching and B-magnitude cuts. Most of the data lie in a parameter space defined from the M31 and Milky Way distribution, indicating that the contamination from background objects in the Gemini data is indeed quite small. The data suggest a clear blue subpopulation with colours $(U - B)_o \sim 0.1$ and $(B - I)_o \sim 1.65$. A red subpopulation is not clearly identified in this colour–colour diagram.

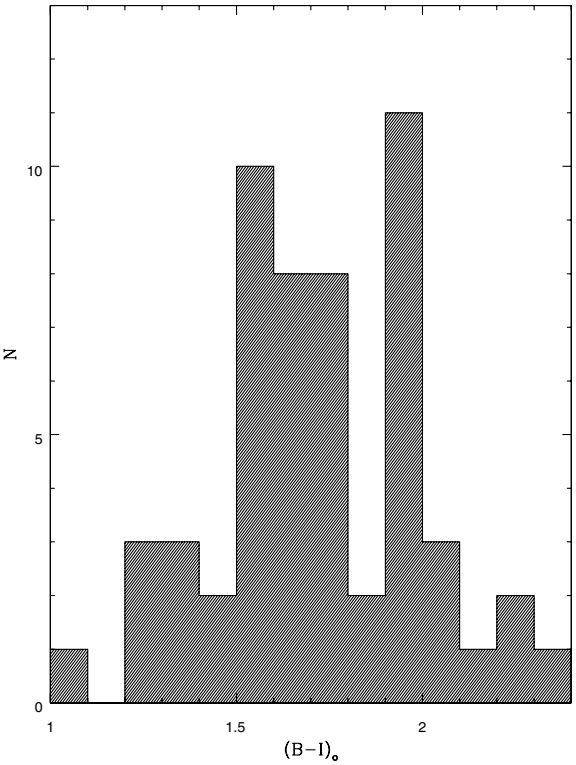

Figure 6. Histogram of $(B-I)_o$ colours for candidate GCs after colour–colour selection from Gemini/GMOS imaging. Two clear peaks are seen. A KMM statistical test confirms peaks at $(B-I)_o = 1.65$ and 1.90 with similar number of GCs in each subpopulation.

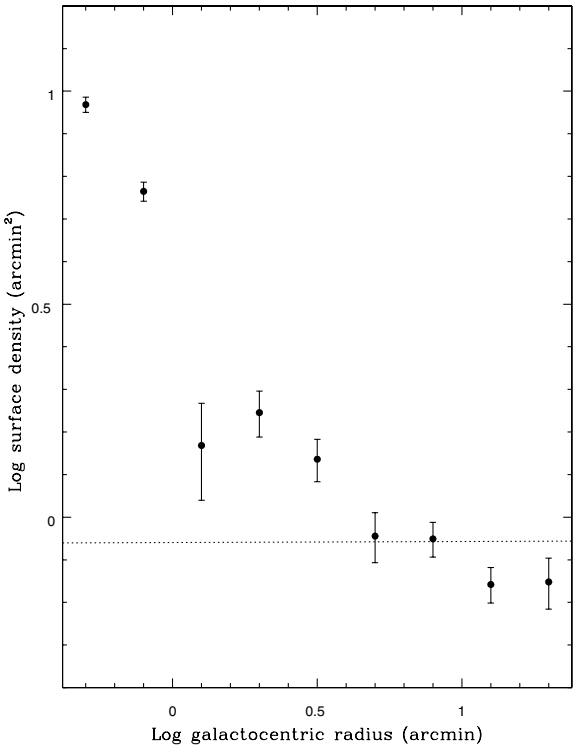

Figure 7. Globular cluster surface density against galactocentric radius for the INT/WFC sample. The dotted line indicates a background region surface density at a radius of greater than 13 arcmin.

in the combined Milky Way and M31 data sets of 0.12 mag, added in quadrature with our typical $(U-B)_o$ photometric error. Most of the data lie in the defined region, indicating that the contamination in the Gemini data is indeed low. The data show a group of blue GCs with values $(U-B)_o \sim 0.1$ and $(B-I)_o \sim 1.65$. A second, red subpopulation is difficult to identify clearly.

If we examine only the $(B-I)_o$ colours of the objects within the colour-selected region, we then obtain the histogram shown in Fig. 6. Visually, and via a KMM statistical test (Ashman, Bird & Zepf 1994), the Gemini GC candidates are clearly bimodal. The peaks are located at $(B-I)_o = 1.65$ and 1.90.

7 LARGE AREA STUDY OF THE NGC 3379 GLOBULAR CLUSTER SYSTEM

In order to extend our study beyond the central few arcmin of NGC 3379 (i.e. that covered by the Gemini imaging), we now return to the INT imaging. We restrict candidate GCs to lie within 5.5 arcmin (18 kpc) in galactocentric radius, as beyond this radius we no longer witness a decline in the surface density of detected objects (see Fig. 7). Thus the majority of objects interior to this radius appear to be associated with NGC 3379. This radial selection also ensures there are very few, if any GCs associated with NGC 3384 (projected separation of 7.2 arcmin) in our final object list.

We then applied the same B-magnitude selection (i.e. $19 < B_o < 23$) as above. The resulting GC candidates in $(U-B)_o$ versus $(B-I)_o$ colour space are shown in Fig. 8. Like the Gemini-selected objects, our large area sample reveals a small number of blue GCs with colours at $(U-B)_o \sim 0.1$, $(B-I)_o \sim 1.65$, but no strong red grouping.

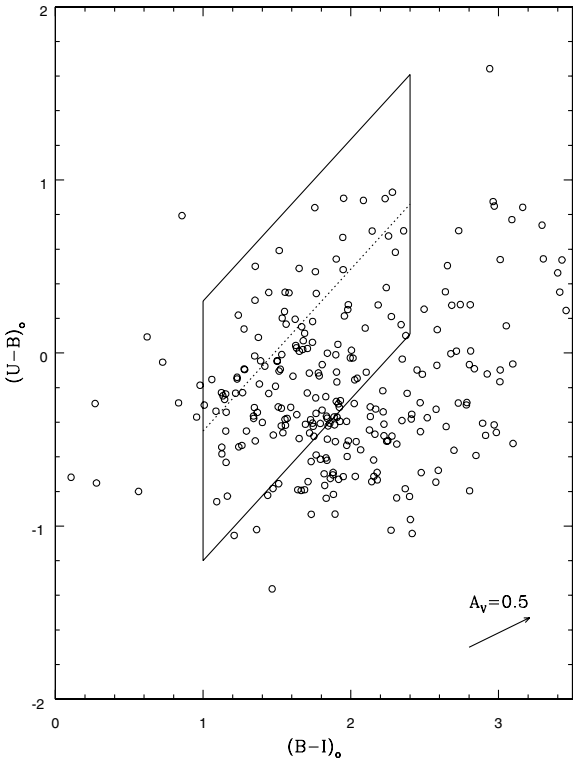

Figure 8. $(U-B)_o$ versus $(B-I)_o$ colour distribution for the candidate GCs from the large area INT images, after applying B-magnitude cuts. The large number of sources with $(U-B)_o \sim -0.5$ are likely to be contaminating background objects.

We find 133 candidate GCs within the colour-selected region. The measured magnitudes and positions of these objects are listed in Appendix A. How does this final number compare with the total number of GCs estimated by Harris & van den Bergh (1981) of 290 $\pm$ 150? Our data have complete radial coverage (with the possibility of missing a few GCs in the very inner regions) but clearly undersample the GC luminosity function. We reach magnitudes similar to, or slightly brighter than, the expected turnover magnitude. Thus crudely we expect a factor of 2–2.5$\times$ more GCs than we detected, i.e. 266–333.

Examination of the colour-selected region, however, suggests that it contains a number of background objects, i.e. objects with a wide range of $(B - I)_o$ colours and a mean $(U - B)_o$ colour of about -0.5. These were not generally seen in the Gemini-selected data, and are presumably not GCs but background galaxies. So the total number of GCs in NGC 3379 may be closer to 250 than 300. Both values are consistent with the low GC specific frequency found by Harris & van den Bergh (1981).

In order to further investigate this issue we have defined a background region of the same central area as studied above but located at a galactocentric radius of more than 13.3 arcmin (44 kpc). The background objects, after B-magnitude selection, are shown in Fig. 9. Indeed, these background objects cover a range in $(B - I)_o$ with a mean $(U - B)_o$ of about -0.5. In Fig. 10 we show the $(B - I)_o$ colour distribution for GC candidates before and after statistical background subtraction. Two GC subpopulations are revealed with peaks around $(B - I)_o \sim 1.65$ and 1.90. As with the Gemini-selected data, the blue subpopulation is easily identified in both colour–colour space and in the $(B - I)_o$ distribution. However, the red subpopulation is only clearly identified in the $(B - I)_o$ distribution.

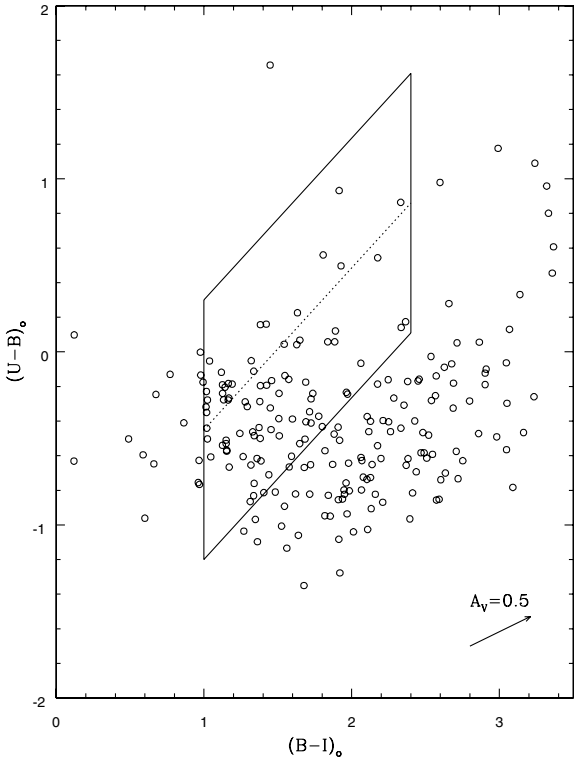

Figure 9. $(U - B)_o$ versus $(B - I)_o$ colour distribution of the background objects, from an area matched to that for Fig. 8. Some of the background objects have colours that fall within the globular cluster selection region.

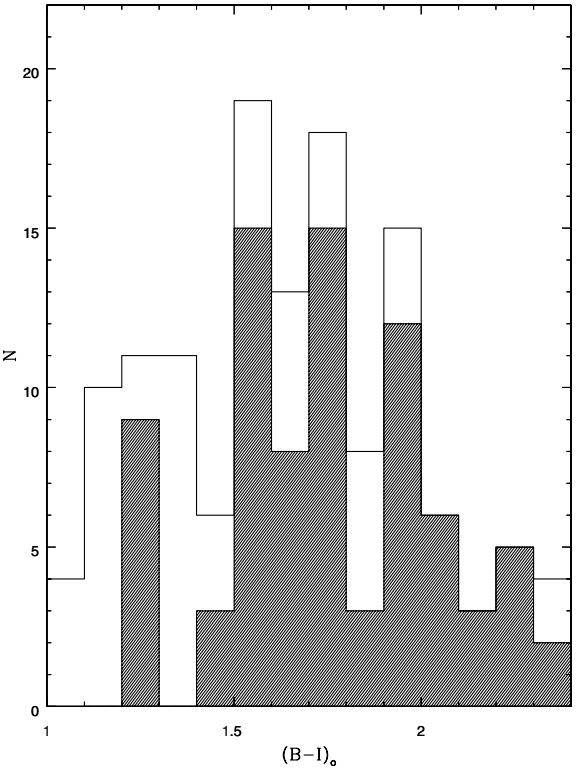

Figure 10. Histogram of $(B - I)_o$ colours for candidate GCs. The open histogram shows the objects within the colour selection region. The shaded histogram shows the distribution after applying a statistical background correction. Both before and after background correction, the histogram shows evidence for two subpopulations at $(B - I)_o \sim 1.65$ and 1.90.

8 GLOBULAR CLUSTER MEAN AGES AND METALLICITIES

In order to interpret our data on NGC 3379 we compare it to similar data for the Milky Way and M31 GC systems. To aid in this interpretation we have created smoothed colour density plots using a Gaussian smoothing kernel. In Fig. 11 we show the density plots for the MW and M31 (i.e. a smoothed version of Fig. 1), with a background-subtracted density plot from the large area coverage of NGC 3379 (i.e. Fig. 7 minus Fig. 8).

We first discuss the Milky Way and M31 GC systems. For the Milky Way, the data reveals the dominant blue subpopulation at $(U - B)_o = 0.04$ and $(B - I)_o = 1.51$, with an uncertainty in the peak location of ± 0.05. The red subpopulation is harder to define as it contains fewer GCs. However, a small enhancement can be seen at $(U - B)_o \sim 0.35$ and $(B - I)_o \sim 1.81$. The distribution for M31 is similar to that for the Milky Way. We estimate the dominant blue subpopulation to be at $(U - B)_o = 0.12$ and $(B - I)_o = 1.62 \pm 0.05$. The red subpopulation appears to have a centre around $(U - B)_o = 0.45$ and $(B - I)_o = 1.90 \pm 0.05$.

An empirical transformation between $(U - B)_o$ and $(B - I)_o$ to [Fe/H] is given by Barmby et al. (2000). Barmby et al. calculated these transformations based on spectroscopic metallicities for $\sim$80 Milky Way GCs. Using these transformations we can calculate 'photometric metallicities' based on our colour estimates. These are summarized in Table 1. The mean metallicity of the two subpopulations from spectroscopy are [Fe/H] = -1.59, -0.55 and -1.40, -0.58 for the Milky Way and M31, respectively (Forbes et al. 2000). Table 1 shows a good

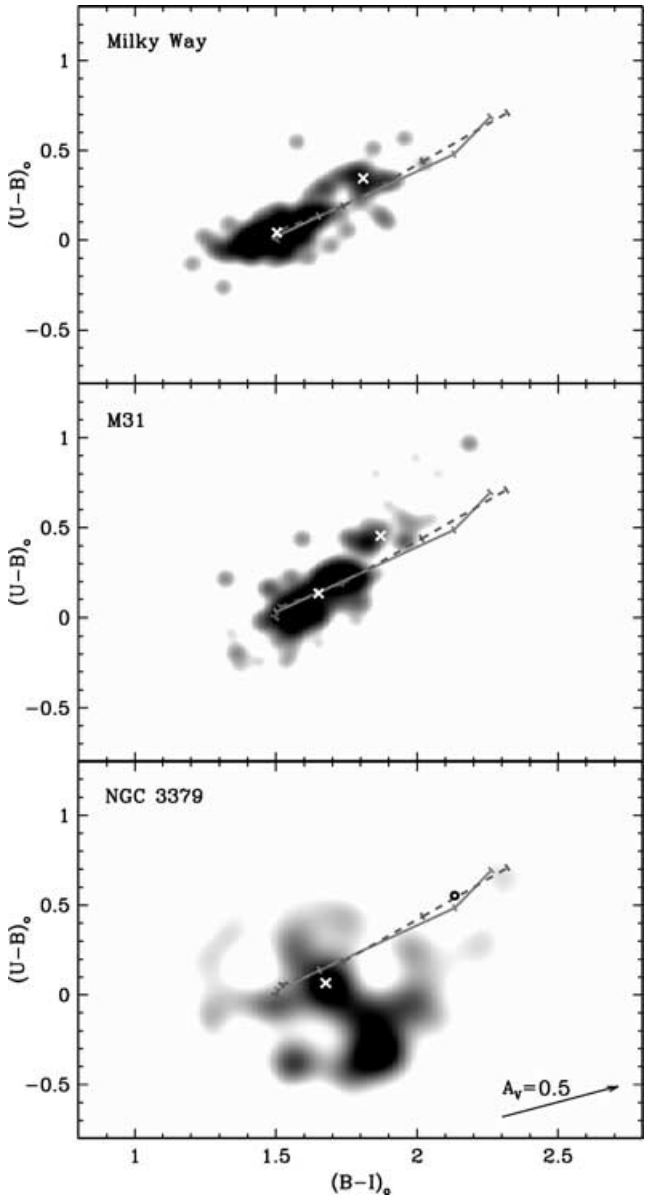

Figure 11. $(U-B)_o$ versus $(B-I)_o$ colour density plot for the Milky Way, M31 and NGC 3379 globular cluster systems. The solid line shows the 15 Gyr old model track from Maraston (private communication) with tick marks for metallicities (from right to left) of [Fe/H] = 0.0, −0.33, −1.35, −2.25. The dashed line shows the 15 Gyr old model track from Brocato et al. (2000) with tick marks for metallicities (from right to left) of [Fe/H] = 0.0, −0.5, −1.3, −1.8, −2.3. The location of the subpopulation mean colours for each galaxy are shown by a white cross (NGC 3379 does not have a clear red subpopulation). The open circle indicates the colours of NGC 3379 galaxy at the effective radius. The high density peak at $(U-B)_o \sim -0.3$ and $(B-I)_o \sim 1.8$ is probably due to faint background galaxies.

correspondence between our photometric and the spectroscopic metallicities.

We find that the mean colours (metallicities) of the M31 GC system are redder (more metal-rich) than that of the of GC system the Milky Way. This is also the situation for the spectroscopically defined metallicities. This is consistent with the mass (luminosity) of the Milky Way being less than that for M31, as per the galaxy luminosity – GC metallicity relation (Forbes & Forte 2001; Larsen et al. 2001).

Table 1. Globular cluster metallicities.

	Spectra	$(U-B)_o$	$(B-I)_o$
Milky Way			
Metal-poor	−1.59	−1.75	−1.73
Metal-rich	−0.55	−0.89	−0.89
M31			
Metal-poor	−1.40	−1.53	−1.42
Metal-rich	−0.58	−0.62	−0.64
NGC 3379			
Metal-poor	–	−1.64	−1.36
Metal-rich	–	–	−0.6

Fig. 11 also includes model tracks from Brocato et al. (2000) and Maraston (private communication) for a 15-Gyr-old single stellar population (SSP). We find that the 15-Gyr-old tracks are closer to the location of the metal-rich subpopulation than say the 12-Gyr, or younger, model tracks (the metal-poor subpopulation is equally well fitted by a 15- or 12-Gyr-old track). Assuming the difference is purely in the $U-B$ colour, the models are too blue by 0.1–0.15 mag. Given a mean age for Milky Way GCs from colour–magnitude diagrams of around 12 Gyr (e.g. Salaris & Weiss 2002), it suggests that these SSP models are not yet on the correct *absolute* age scale. The tracks show a range of metallicities for a 15-Gyr-old population. The Milky Way blue subpopulation has a peak close to a metallicity of [Fe/H] = −1.5, with the M31 blue GCs between [Fe/H] = −1.5 and −1.0. For both galaxies, the red subpopulation lies between [Fe/H] = −0.3 and −1.3.

We have also compared the SSP models of Worthey (1994) with our data and find that the Worthey models fall well below the location of the metal-rich subpopulation for any age. A detailed comparison between the various stellar population models is beyond the scope of this paper. However, the origin of the large differences between the $U-B$ colours of the Worthey models, and those of Brocato et al. and Maraston, seem to lie in a combination of the theoretical isochrones adopted (those from Vandenberg & Bell 1985; Green, Demarque & King 1987, in the case of the Worthey models) and the conversion between luminosity/temperature to magnitude/colour in the observational plane. The Worthey models achieved this by multiplying observed stellar fluxes by empirical filter transmission functions, whilst Maraston employ a combination of empirical and theoretical colour–temperature relations (see Maraston 1998). As discussed by Brocato et al. (2000), variations in other model ingredients such as the initial mass function (IMF) slope and low-mass cut-off do not significantly affect the predicted integrated colours. In any event, regardless of the specific origin of these discrepancies, we conclude that the $U-B$ colours of the Worthey models do not accurately reflect the colours of globular clusters.

Turning now to NGC 3379. The colour density plot for NGC 3379 clearly shows a blue GC subpopulation near $(U-B)_o = 0.08 \pm 0.05$ and $(B-I)_o = 1.64 \pm 0.05$. The plot also shows some remaining galaxy contamination with $(U-B)_o \sim -0.3$. The colours of these objects are consistent with late-type spirals and blue compact dwarfs (Schroeder & Visvanathan 1996). A red GC subpopulation is not obvious; it is only revealed when the distribution in $(B-I)_o$ colour only is examined (see also Figs 5 and 9). We believe this is due to the larger mean error in our $U-B$ colours for the metal-rich subpopulation (although the presence of an intermediate-aged population could also contribute). From the colour–magnitude diagram (Fig. 4), it can be seen that the red subpopulation is fainter on average by about half a magnitude than the blue one (this is

presumably due to additional line blanketing in the more metal-rich GCs). Larsen et al. (2001) also found evidence for the red GCs being systematically fainter than the blue ones. For their small sample of 21 blue and 24 red GCs, they estimated V-band turnover magnitudes of 22.57 for the blue GCs and 23.02 for the red GCs. For NGC 3379, this results in an additional colour error of $\sim$0.3 mag for the metal-rich subpopulation. This effect may be spreading out the (fainter) metal-rich subpopulation. Our $B-I$ colour errors are generally half those in $U-B$, and hence are less affected. If we consider $(B-I)_o$ colour only, i.e. the histograms of Figs 6 (Gemini selected) and 10 (INT selected), then we estimate that the red subpopulation has a mean colour of $(B-I)_o \sim 1.9$.

The intrinsic $U-B$ and $B-I$ colours of the blue subpopulation in NGC 3379 are intermediate between those of the Milky Way and M31 GC systems. The Barmby et al. (2000) transformation leads to a photometric metallicity of [Fe/H] $= -1.64 \pm 0.14$ from $(U-B)_o$ and -1.36 ± 0.14 from $(B-I)_o$ for the blue subpopulation. This is consistent with the metallicity indicated by the Maraston ([Fe/H] ~ -1.35) and Brocato et al. ([Fe/H] ~ -1.5) 15 Gyr SSP tracks. The photometric metallicity for the red subpopulation, based on $(B-I)_o$ colour only, is estimated to be [Fe/H] ~ -0.6. These values are summarized in Table 1.

The ages of the GC subpopulations in NGC 3379 are less well constrained by our data. However, similarities between NGC 3379 and the Milky Way and M31 GC colours suggests that the blue subpopulation in all three galaxies has a similar, old age. From the colour–magnitude diagram of Fig. 4, the red subpopulation in NGC 3379 is fainter in the mean than the blue GCs. This effectively rules out a young (i.e. $<$3 Gyr) age.

9 CONCLUSIONS

Magnitudes and colours, from the Isaac Newton Telescope, for 133 candidate globular clusters around NGC 3379 are presented. Our detection rate is consistent with a low specific frequency. These candidates, and a subsample selected from imaging with the Gemini North Telescope, reveal evidence for a blue and red subpopulation.

We have compared the $(U-B)_o$ versus $(B-I)_o$ colours of the NGC 3379 globular cluster system with that for the Milky Way and M31. The Milky Way and M31 reveal similar GC colour distributions, although with slightly different slopes (which may simply be the result of uncertain reddening corrections). The metal-poor and metal-rich subpopulations can be seen as a dominant blue and a less well-defined red peak. Using the single stellar population models of Maraston (private communication) and Brocato et al. (2000), we find that the mean colours of both subpopulations are best reproduced by their 15-Gyr-old tracks. Even so, small colour differences between the model and the measurements exist. As the mean age of the Milky Way globular clusters is thought to be closer to 12 Gyr, it suggests that these model require a relative age adjustment. The estimated mean metallicities of the two subpopulations are very similar to those measured previously from spectroscopy. We also investigated the models of Worthey (1994), and found they were unable to reproduce the $(U-B)_o$ colour of the metal-rich subpopulation in M31 and the Milky Way for any age.

For NGC 3379 we detect a blue subpopulation with very similar $(U-B)_o$ and $(B-I)_o$ colours, and presumably age/metallicity, to that of the Milky Way and M31 globular cluster systems. Thus the blue GCs in NGC 3379 are consistent with being very old and with a mean metallicity of [Fe/H] ~ -1.5. The red subpopulation is less well-defined, perhaps due to increased photometric errors, but has a similar mean $(B-I)_o$ colour to the Milky Way and M31 globular cluster systems. This implies a mean photometric metallicity of [Fe/H] ~ -0.6.

ACKNOWLEDGMENTS

We thank M. Pierce and J. Strader for useful comments. We also thank A. Terlevich for his help in observing and the initial data reduction. The data used in this project were obtained with Isaac Newton Telescope at La Palma Observatory and the Gemini North Telescope. This research has made use of the NASA/IPAC Extragalactic Data base (NED) which is operated by the Jet Propulsion Laboratory, California Institute of Technology, under contract with the National Aeronautics and Space Administration.

REFERENCES

Ajhar E. A., Blakeslee J. P., Tonry J. L., 1994, AJ, 108, 2087
Ashman K. M., Zepf S. E., 1992, ApJ, 384, 50
Ashman K. A., Bird C. M., Zepf S. E., 1994, AJ, 108, 2348
Barmby P., Huchra J. P., Brodie J. P., Forbes D. A., Schroder L. L., Grillmair C. J., 2000, AJ, 119, 727
Beasley M. A., Baugh C. M., Forbes D. A., Sharples R. M., Frenk C. S., 2002, MNRAS, 333, 383
Beasley M. A., Forbes D., Brodie J., Kissler-Patig M., 2003, MNRAS, submitted
Bridges T. J., Ashman K. M., Zepf S. E., Carter, D., Hanes D. A., Sharples R. M., Kavelaars J. J., 1997, MNRAS, 284, 376
Brocato E., Castellani V., Poli F., Raimondo G., 2000, A&AS, 146, 91
Cote P., Marzke R. O., West M. J., 1998, ApJ, 501, 554
Forbes D. A., Forte J. C., 2001, MNRAS, 322, 257
Forbes D. A., Thomson R. C., 1992, MNRAS, 254, 723
Forbes D. A., Brodie J. P., Huchra J., 1997, AJ, 113, 887
Forbes D. A., Masters K. L., Minniti D., Barmby P., 2000, A&A, 358, 471
Forbes D. A., Beasley M. A., Brodie J. P., Kissler-Patig M., 2001, ApJ, 563, L143
Geisler D., Lee M. G., Kim E., 1996, AJ, 111, 1529
Green E. M., Demarque P., King C. R., 1987, The Revised Yale Isochrones and Luminosity Functions. Yale Observatory, New Haven
Harris W. E., 1996, AJ, 112, 1487
Harris W. E., van den Bergh S., 1981, AJ, 86, 1981
Kissler-Patig M., Gebhardt K., 1998, AJ, 116, 2237
Kissler-Patig M., Brodie J. P., Schroder L. L., Forbes D. A., Grillmair C. J., Huchra J. P., 1998, AJ, 115, 105
Kundu A., Whitmore B. C., 2001, AJ, 122, 1251
Landolt A. U., 1992, PASP, 104, 336
Larsen S. S., Brodie J. P., Huchra J. P., Forbes D. A., Grillmair C. J., 2001, AJ, 121, 2974
Larsen S. S., Brodie J. P., Beasley M. A., Forbes D. A., 2002, AJ, 124, 828
Maraston C., 1998, MNRAS, 300, 872
Puzia T. H., Zepf S. E., Kissler-Patig M., Hilker M., Minniti D., Goudfrooij P., 2002, A&A, 391, 453
Rejkuba M., 2001, A&A, 369, 812
Salaris M., Weiss A., 2002, A&A, 388, 492
Secker J., Geisler D., McLauglin D. E., Harris W. E., 1995, AJ, 109, 1019
Schroeder A., Visvanathan N., 1996, A&AS, 1181, 441
Vandenberg D. A., Bell R. A., 1985, ApJS, 58, 561
Whitmore B. C., Sparks W. B., Lucas R. A., Macchetto F. D., Biretta J. A., 1995, ApJ, 454, L73
Worthey G., 1994, ApJS, 95, 107

APPENDIX A

Table A1 lists the positions and colours of the candidate globular clusters in NGC 3379 identified in this study.

Table A1. Candidate Globular Clusters around NGC 3379.

ID	RA (J2000)	Dec. (J2000)	U (mag)	B (mag)	R (mag)	I (mag)	$B-I$ (mag)
001	10:48:11.36	+12:34:32.14	20.18	20.17	18.79	18.16	2.00
002	10:48:11.22	+12:35:42.37	21.93	22.30	20.96	20.46	1.84
003	10:48:10.99	+12:33:50.10	20.92	21.29	20.02	19.41	1.89
004	10:48:10.04	+12:35:09.40	21.28	21.66	20.65	19.94	1.73
005	10:48:06.50	+12:37:57.63	22.36	21.68	20.25	19.43	2.25
006	10:48:06.36	+12:36:10.70	22.18	22.58	21.42	20.84	1.74
007	10:48:06.35	+12:35:33.91	22.33	22.66	21.29	20.86	1.80
008	10:48:05.74	+12:34:17.05	21.34	21.65	20.43	19.73	1.92
009	10:48:05.61	+12:37:15.56	23.08	22.98	21.13	20.60	2.37
010	10:48:05.28	+12:33:07.97	21.08	21.56	20.62	20.08	1.48
011	10:48:05.22	+12:36:48.93	21.16	21.62	20.65	20.09	1.54
012	10:48:04.74	+12:38:16.43	22.41	23.00	21.73	21.87	1.13
013	10:48:04.44	+12:34:12.39	21.62	21.67	20.55	20.28	1.39
014*	10:48:04.33	+12:35:41.48	23.18	22.69	21.38	20.75	1.95
015*	10:48:04.09	+12:38:36.88	20.54	20.85	19.85	19.34	1.51
016	10:48:03.19	+12:38:56.00	22.83	22.69	21.24	21.41	1.28
017	10:48:03.17	+12:34:36.48	20.32	20.66	19.92	19.57	1.09
018	10:48:02.40	+12:39:12.83	22.53	22.95	21.73	21.39	1.56
019	10:48:01.77	+12:32:48.29	21.77	22.02	20.80	20.19	1.83
020*	10:48:01.68	+12:35:59.72	21.81	21.66	20.56	19.99	1.67
021	10:48:01.59	+12:32:39.15	22.15	22.60	21.84	21.30	1.29
022	10:48:01.23	+12:34:20.79	23.14	22.80	21.82	21.03	1.77
023	10:48:01.01	+12:34:16.68	23.27	22.89	21.78	20.65	2.24
024	10:48:00.74	+12:39:26.23	21.25	21.55	20.76	20.54	1.01
025	10:48:00.57	+12:33:41.88	22.77	23.00	21.89	21.73	1.27
026*	10:48:00.28	+12:32:50.55	21.53	21.67	20.35	19.63	2.04
027*	10:47:58.61	+12:33:57.32	22.85	22.50	21.72	20.94	1.55
028	10:47:58.29	+12:39:34.80	22.29	22.38	21.63	21.10	1.28
029	10:47:57.68	+12:32:08.49	21.71	22.25	21.48	21.01	1.24
030*	10:47:57.64	+12:34:29.41	23.34	22.84	21.83	21.49	1.35
031*	10:47:56.56	+12:33:29.09	21.06	21.16	20.02	19.63	1.52
032	10:47:56.51	+12:32:09.45	21.51	22.37	21.73	21.28	1.09
033	10:47:55.19	+12:30:37.16	22.71	22.76	21.76	21.25	1.50
034	10:47:55.16	+12:30:21.77	20.19	20.53	19.79	19.38	1.16
035	10:47:55.13	+12:32:05.35	21.38	21.69	21.01	20.10	1.59
036*	10:47:54.21	+12:38:36.91	23.08	22.78	21.98	21.43	1.35
037*	10:47:53.97	+12:36:32.31	22.36	21.69	20.47	19.75	1.95
038*	10:47:53.91	+12:34:54.28	23.25	22.66	21.50	21.14	1.52
039	10:47:53.81	+12:31:09.03	20.05	20.28	19.49	19.16	1.12
040	10:47:53.75	+12:32:56.42	20.60	20.89	19.66	18.98	1.91
041*	10:47:53.74	+12:33:48.33	22.47	22.27	21.09	20.65	1.62
042*	10:47:53.48	+12:34:55.67	21.88	21.67	20.68	20.14	1.53
043*	10:47:53.32	+12:34:14.15	22.61	22.62	21.44	20.72	1.90
044*	10:47:53.29	+12:35:05.76	23.23	22.53	21.01	20.38	2.14
045*	10:47:52.46	+12:36:00.51	23.14	22.25	20.75	20.02	2.23
046	10:47:51.71	+12:32:52.10	22.78	22.89	21.58	20.79	2.10
047	10:47:51.37	+12:40:08.89	22.24	22.73	21.56	21.08	1.65
048*	10:47:50.99	+12:35:49.78	20.78	20.75	19.53	19.05	1.71
049	10:47:50.75	+12:30:22.69	21.93	22.17	21.24	20.73	1.44
050*	10:47:50.68	+12:35:30.07	21.49	21.31	20.13	19.57	1.74
051*	10:47:50.56	+12:35:32.43	21.57	21.35	20.15	19.39	1.96
052*	10:47:50.47	+12:35:19.56	22.49	22.44	21.37	20.53	1.91
053*	10:47:50.43	+12:34:37.76	22.18	21.83	20.65	20.39	1.44
054*	10:47:50.42	+12:33:49.17	22.53	22.04	20.84	20.39	1.65
055	10:47:50.26	+12:32:22.91	21.59	22.41	21.30	21.25	1.16
056	10:47:50.10	+12:31:06.72	22.42	22.76	21.75	21.39	1.37
057*	10:47:49.67	+12:34:33.57	20.22	20.11	18.88	18.42	1.69
058*	10:47:49.66	+12:34:11.20	22.82	22.24	20.80	19.94	2.30
059*	10:47:48.96	+12:35:23.11	21.50	21.66	20.68	20.43	1.23

Table A1 – *continued*

ID	RA (J2000)	Dec. (J2000)	U (mag)	B (mag)	R (mag)	I (mag)	$B-I$ (mag)
060	10:47:48.60	+12:37:03.83	21.72	21.77	20.79	20.27	1.50
061	10:47:48.59	+12:35:32.40	20.98	21.15	20.25	19.77	1.38
062*	10:47:48.20	+12:35:45.07	21.59	21.70	20.45	19.98	1.72
063*	10:47:48.00	+12:35:07.78	21.29	21.67	20.38	20.10	1.57
064*	10:47:47.91	+12:34:38.75	21.94	22.34	20.86	20.94	1.40
065*	10:47:47.90	+12:36:22.85	23.01	22.79	21.82	21.55	1.24
066*	10:47:47.87	+12:35:05.17	21.61	21.54	20.41	19.86	1.68
067*	10:47:47.80	+12:34:15.41	22.84	21.94	20.51	19.99	1.95
068*	10:47:47.78	+12:36:41.23	21.62	21.90	20.73	20.00	1.90
069	10:47:47.40	+12:37:19.00	22.38	22.63	21.81	20.87	1.76
070*	10:47:47.30	+12:34:05.47	22.86	22.59	21.39	20.60	1.98
071	10:47:46.85	+12:36:52.44	21.85	22.21	21.50	20.87	1.34
072	10:47:46.78	+12:31:37.35	21.92	22.34	22.11	20.81	1.53
073	10:47:46.48	+12:32:34.57	22.12	22.50	21.38	21.16	1.34
074	10:47:46.30	+12:31:19.99	21.95	21.86	20.73	20.49	1.37
075	10:47:46.22	+12:38:49.41	20.19	20.61	19.33	18.87	1.75
076*	10:47:45.79	+12:34:48.40	21.99	21.99	20.63	20.15	1.84
077*	10:47:45.65	+12:34:51.91	21.73	22.00	20.79	20.07	1.93
078	10:47:45.54	+12:40:08.99	20.81	21.32	20.42	19.97	1.35
079	10:47:45.44	+12:31:33.17	21.57	21.80	21.03	20.58	1.22
080	10:47:45.19	+12:39:57.83	21.40	21.65	20.89	20.52	1.13
081	10:47:43.76	+12:30:45.96	20.07	20.18	19.09	18.40	1.78
082*	10:47:43.67	+12:33:34.16	22.32	22.47	21.26	21.41	1.06
083*	10:47:43.55	+12:37:04.17	22.20	22.34	21.35	21.11	1.23
084*	10:47:43.34	+12:36:46.37	22.58	22.34	21.09	20.79	1.55
085*	10:47:42.25	+12:34:47.47	22.51	22.49	21.30	20.82	1.67
086	10:47:42.14	+12:35:08.62	21.99	22.62	21.87	21.46	1.15
087*	10:47:42.11	+12:36:10.11	22.31	22.34	21.14	20.34	2.00
088*	10:47:41.84	+12:35:40.68	23.10	22.26	21.12	20.50	1.76
089*	10:47:41.30	+12:36:50.81	22.91	22.87	21.80	21.24	1.63
090	10:47:40.91	+12:31:37.45	21.54	22.08	21.51	20.81	1.26
091*	10:47:40.82	+12:34:05.12	22.01	22.47	21.29	20.75	1.72
092	10:47:40.80	+12:39:42.82	21.54	21.86	20.68	20.33	1.53
093	10:47:40.73	+12:32:17.44	19.61	19.70	18.79	18.42	1.28
094	10:47:40.61	+12:38:57.95	19.74	19.93	18.98	18.44	1.49
095*	10:47:40.61	+12:35:22.13	20.50	20.60	19.59	19.09	1.51
096*	10:47:40.60	+12:35:53.78	20.94	20.91	19.87	19.28	1.63
097	10:47:40.51	+12:37:22.36	22.43	22.26	21.05	20.70	1.56
098	10:47:40.03	+12:34:36.04	22.68	22.83	21.57	20.80	2.03
099*	10:47:39.71	+12:33:58.78	22.64	22.17	20.98	20.41	1.76
100*	10:47:39.70	+12:32:26.12	20.82	20.76	19.55	19.02	1.74
101	10:47:39.47	+12:35:37.17	21.30	21.75	20.85	20.60	1.15
102	10:47:39.44	+12:39:37.58	22.54	22.26	20.96	20.08	2.18
103	10:47:39.33	+12:30:53.43	22.11	21.90	20.33	19.63	2.27
104	10:47:39.32	+12:39:42.28	21.91	22.14	21.15	20.43	1.71
105	10:47:39.24	+12:35:35.50	21.49	21.91	20.87	20.21	1.69
106*	10:47:39.24	+12:35:01.26	23.30	22.95	21.53	21.37	1.58
107	10:47:39.01	+12:36:45.95	22.66	22.52	21.37	20.42	2.10
108	10:47:38.98	+12:35:26.48	22.84	22.68	21.10	20.34	2.34
109	10:47:38.89	+12:39:38.32	22.50	22.50	21.91	20.97	1.53
110	10:47:38.60	+12:35:57.03	22.01	22.42	21.39	20.62	1.79
111	10:47:38.31	+12:31:53.19	21.45	21.44	20.28	19.79	1.65
112*	10:47:38.28	+12:35:10.56	21.96	22.44	21.17	20.69	1.75
113	10:47:38.21	+12:39:28.19	20.90	20.98	20.00	19.56	1.42
114	10:47:37.84	+12:31:04.88	22.59	22.70	21.19	20.80	1.90
115	10:47:37.76	+12:33:33.40	21.32	21.07	19.75	19.09	1.98
116*	10:47:37.66	+12:34:14.78	21.80	21.82	21.32	20.47	1.35
117	10:47:37.49	+12:38:56.74	22.23	22.77	22.28	21.65	1.13
118	10:47:37.34	+12:36:02.54	21.61	21.96	20.66	20.33	1.63
119*	10:47:37.14	+12:35:21.82	22.00	22.03	20.80	20.02	2.01
120	10:47:36.91	+12:37:21.02	21.81	20.93	19.46	18.84	2.09
121	10:47:36.35	+12:34:41.33	20.08	20.35	19.57	19.20	1.14
122	10:47:36.06	+12:35:53.02	22.10	22.23	21.08	20.63	1.61

Table A1 – *continued*

ID	RA (J2000)	Dec. (J2000)	U (mag)	B (mag)	R (mag)	I (mag)	$B-I$ (mag)
123	10:47:36.05	+12:39:12.20	21.92	21.22	19.53	18.86	2.36
124	10:47:35.89	+12:30:45.05	21.96	22.03	20.77	20.22	1.81
125	10:47:35.35	+12:38:47.74	21.49	21.81	21.25	20.46	1.35
126*	10:47:34.01	+12:33:27.75	21.21	20.29	18.66	18.00	2.28
127*	10:47:33.83	+12:34:43.89	23.07	22.53	21.17	20.62	1.90
128	10:47:33.62	+12:34:38.74	21.16	21.33	20.14	19.42	1.91
129	10:47:33.51	+12:33:08.65	21.03	21.38	20.18	19.62	1.76
130	10:47:32.63	+12:36:26.46	21.43	21.67	21.13	20.51	1.15
131	10:47:32.27	+12:36:59.72	20.95	21.09	19.91	19.30	1.79
132	10:47:31.83	+12:36:56.07	21.87	22.25	21.08	20.70	1.55
133	10:47:31.44	+12:35:53.33	20.07	20.45	19.29	18.61	1.84

Notes:* = Globular cluster present in the Gemini selected object lists. Galaxy centre is RA = 10:47:49.6, Dec. = +12:34:55 (J2000).

This paper has been typeset from a TEX/LATEX file prepared by the author.